Materials Today Communications 55 (2026) 115810

Contents lists available at ScienceDirect

Materials Today Communications

journal homepage: www.elsevier.com/locate/mtcomm

Exploring complex-forming corrosion inhibitors to reduce stiction in non-asbestos organic friction materials

Michele Motta [a,*], Agusti Sin [b,c], Lorenzo Fedrizzi [a], Francesco Andreatta [a]

[a] University of Udine, Polytechnic department of engineering and architecture, Via del Cotonificio 108, Udine 33100, Italy
[b] ITT, Friction Technologies, Via Molini 19, Barge, CN 12032, Italy
[c] Joint Lab ITT, UniTO, via Quarello 15, Torino, TO 101135, Italy

ARTICLE INFO

Keywords:
Gray cast iron
Corrosion inhibitors
Sodium oxalate
2,5-pyridinedicarboxylic acid
Stiction

ABSTRACT

The increasing adoption of electric and hybrid vehicles (BEVs, HEVs, PHEVs) drives significant changes in braking system design, introducing durability challenges related to corrosion. Specifically, stiction between Non-Asbestos Organic (NAO) friction materials and gray cast iron discs represents a critical issue effecting the braking reliability. This study investigates complex-forming organic corrosion inhibitors, 2,5-pyridinedicarboxylic acid and sodium oxalate, as potential additives to mitigate this phenomenon. First, the inhibition mechanisms were examined by evaluating the corrosion behavior of gray cast iron discs in an electrolyte solution simulating the disc–friction material crevice. In the second part of the study, a dedicated stiction test procedure was employed to reproduce stiction phenomena in a simulated brake assembly. After identifying a friction material formulation exhibiting high stiction susceptibility, the influence of the investigated inhibitors on stiction forces and on the morphological characteristics of both disc and pad surfaces was evaluated by introducing the inhibitors into the electrolyte solution. Based on the obtained results, additional friction material formulations containing sodium oxalate as an additive at different concentrations of 4 and 6%$_w$ were produced and experimentally characterized.

1. Introduction

The braking system of a vehicle is typically composed of several components, the most critical of which are the caliper, the disc, and the brake pads. In commercial vehicles, the disc is commonly made of gray cast iron containing type A graphite flakes embedded in a pearlitic matrix. This material offers numerous advantages, including low production costs, excellent tribological performance, high thermal conductivity, and good damping capacity [1]. However, due to the galvanic coupling between the iron matrix and the graphite phase, gray cast iron is susceptible to corrosion phenomena that can potentially impair the reliability of the braking system. Rust accumulation during prolonged stationary periods of the vehicle can cause the static friction phenomenon, commonly referred to as "stiction," brake judder, and stick-slip [2–4]. In addition to the use of metallic zinc and pH-buffering agents [5–7], corrosion inhibitors are emerging as a promising alternative for mitigating corrosion phenomena in gray cast iron discs [8–11]. Pyridine derivatives in particular represent a highly promising class of corrosion inhibitors for iron and steel in acidic environments, with their inhibition efficiency being extensively demonstrated in the literature [8,12–22]. Physical and chemical interactions were reported to be involved in the inhibition mechanism [21,23].

Carboxylic acid salts represent another interesting class of corrosion inhibitors. Carboxylates are generally considered non-oxidizing corrosion inhibitors [24]. For iron and mild steel, the establishment of passivity in solutions containing carboxylic acids has been shown to depend on the presence of dissolved oxygen [25]. Reinhard et al. [25] reported that iron passivation in air-saturated aqueous solutions of salts of weak carboxylic acids occurs only when the solution pH lies outside the buffering range of the corresponding conjugate acid–base pair. Under these conditions, Fe^{2+} ions generated during the corrosion process are retained within the electrochemical double layer and are rapidly oxidized to Fe^{3+}, leading to the formation of a passive oxide layer.

The stability of this passive film is further enhanced by the formation of intermediate complex species that adsorb onto the metal surface [25–27]. In this context, carboxylate ions are believed to act preferentially at local defects in the oxide film, where corrosion is mitigated through a pore-plugging mechanism involving poorly soluble ferric compounds. This effect may be further complemented by the direct adsorption of carboxylates onto the passive film [24]. Sodium oxalate in

* Corresponding author.
E-mail address: michele.motta@uniud.it (M. Motta).

https://doi.org/10.1016/j.mtcomm.2026.115810
Received 16 June 2026; Received in revised form 21 July 2026; Accepted 26 July 2026
Available online 27 July 2026

this regard is an interesting compound, as it is highly available, also from natural resources such as plants and vegetables, or as a metabolic product of microorganisms such as *Aspergillus niger* [26,28]. It is commonly used in anodization [29,30], and as a corrosion inhibitor [31–36]. Goidanich et al. [37] also proposed the use of bio-passivation treatments as new anti-corrosive treatments to improve the corrosion resistance of Corten steel using *Beauveria bassiana* as a fungal strain capable of forming a passive layer containing oxalate.

The use of pyridine dicarboxylic acids can combine the inhibitive properties of pyridine derivatives and the carboxylic group. The possibility of using these compounds as organic corrosion inhibitors were comprehensively studied by Hassan et al. [22]. Chemisorption and the formation of complexes were further reported in several papers [38].

Because of the excellent adsorption properties reported for iron-based material [22,38], and the capacity of forming complexes with iron ions [39], 2,5-pyridinedicarboxylic acid (2,5-PDA) was selected in this work as a candidate corrosion inhibitor for gray cast iron. Its ability to reduce gray cast iron corrosion was characterized using electrochemical techniques and free immersion analysis and compared to the simplest dicarboxylic acid, sodium oxalate.

Finally, the effect of 2,5-PDA and oxalic acid on the stiction phenomenon was assessed using the stiction test, a procedure specifically designed to generate the stiction phenomenon in the laboratory [40].

2. Experimental procedure

2.1. Materials

Gray cast iron brake discs with the average composition based on XRF analysis, reported in Table 1, were provided by ITT Inc. (ITT-Friction Technologies, Barge, Italy).

37%$_w$ HCl was purchased from Sigma-Aldrich and appropriately diluted to prepare a 0.1 M HCl solution that was used as electrolytic solution in the absence (blank) and in the presence of inhibitors. This solution was selected to simulate the acidic environment within the occluded cell formed at the friction material/disc interface in automotive braking systems. Indeed, the assumption of local acidification at the pad-disc interface is strongly supported by vehicle tests and in-service evidence. In light of this, studying the effect of the inhibitors in an acidic environment is very important to understand their behavior under the critical conditions leading to stiction in service.

2,5-PDA (98% purity), and sodium oxalate $Na_2C_2O_4$ (99.5% purity, powder form) were both procured from Sigma-Aldrich and used as received without further purification. The aim of this study is to evaluate the feasibility of using complexing inhibitors for gray cast iron discs in automotive braking systems. The inhibitor is intended to be included in the formulation of the friction material. In such applications, controlling the release of the inhibitor from the friction material is inherently challenging and, although technical solutions exist, they are proprietary and cannot be disclosed. Therefore, a comparative approach was adopted, in which a blank solution without inhibitors was prepared and compared with solutions containing 2,5-PDA or sodium oxalate at an equal concentration of 0.02 M.

2.2. Electrochemical measurements

Time-dependent potentiodynamic polarization curves were recorded to obtain preliminary information regarding the ability of 2,5-PDA and sodium oxalate to act as organic corrosion inhibitors for gray cast iron. Specifically, potentiodynamic polarization measurements were performed after 10 min, 6 h, and 24 h of immersion in the electrolyte with and without (blank) the inhibitor to study the variation of the inhibition efficiency with the time of immersion. All polarization measurements were acquired using an IPS Elekroniklabor PGU-MOD−200 mA electrochemical workstation (measurement resolution/uncertainty for potential and current is $< \pm 0.01\%$, with an internal ADC potential resolution of 1 μV and a minimum current resolution of 100 pA). Electrochemical measurements were conducted using a three-electrode setup. The gray cast iron samples were used as working electrodes (WE), a graphite bar was the counter electrode (CE), and a 3 M KCl Ag/AgCl electrode was employed as the reference electrode (RE). All measurements were carried out using an electrochemical cell designed to expose a 1 cm^2 area of the working electrode to the electrolyte. A PTFE gasket ensured proper sealing, and a copper strip was used to electrically connect the non-exposed surface of the working electrode to the electrochemical workstation.

The gray cast iron samples were polished up to grit 2000 and cleaned in ethanol and rinsed with deionised water before every measurement. The potential was scanned with a scan rate of 0.2 mVs^{-1} from −0.75–0.00 V vs. the RE potential. Cathodic and anodic scans were obtained separately and for a minimum of three repetitions for each solution. The inhibition efficiency at the different times of immersion was calculated according to the equation:

$$\eta = (1 - \frac{I_{inh}}{I_0}) \cdot 100$$

where I_{inh} is the corrosion current density in the presence of the inhibitors in the electrolyte solution, while I_0 is the current density in the electrolyte without inhibitors.

Electrochemical impedance spectroscopy (EIS) was performed using the same electrolyte solutions and experimental setup by means of an Autolab PGSTAT 30 potentiostat (potential resolution of 30 μV and current resolution of 0.0003% of the selected current range) at OCP in the frequency range from 1 kHz to 0.01 Hz (8 points per decade), applying a sinusoidal perturbation of 10 mV_{rms} amplitude. The impedance spectra of 3 gray cast iron disc samples immersed in a 0.1 M HCl solution in the presence of the inhibitors were monitored up to 15 days of immersion.

2.3. Morphological and chemical analyses

The morphology and the surface chemical composition of the gray cast iron disc after the impedance measurements were evaluated by means of an optical stereo-microscope (ZEISS SteREO Discovery.V12) and a field-emission microscope (FE-SEM Jeol USA JSM-7600F) equipped with energy dispersive X-ray spectroscopy (EDS Oxford), which was employed for the acquisition of images using secondary electrons and elemental maps to study the interaction of the inhibitor with the gray cast iron. For the visual and chemical observation of the gray cast iron disc submerged in the solution containing 2,5-PDA, different gray cast iron disc samples were employed for the visual and chemical assessments at 7 days and the electrochemical impedance spectroscopy measurements. This was performed to maintain the integrity of the impedance measurements. Conversely, the specimens subjected to the 15-day electrochemical monitoring, in the presence of 2,5-PDA and sodium oxalate, were subsequently utilized for morphological and chemical characterization.

Confocal Raman spectrometer XploRa PLUS (HORIBA Scientific), employing a green laser (532 nm), a 1200 grating, and a 50X LWD

Table 1
Chemical composition of the gray cast iron disc provided by ITT Inc.

Element	Fe	C	Si	Cu	Mn	Cr	S	P	Other elements	TOT
%$_w$	94.4	2.7	1.6	0.12	0.8	0.07	0.06	0.04	0.21	100

objective, was used to obtain information regarding the composition of the protective layers formed on the samples submerged in the different electrolyte solutions containing 2,5-PDA and sodium oxalate. The spectral uncertainty was controlled via a mandatory daily calibration using a standard silicon single-crystal reference (peak at 520.6 cm^{-1}), maintaining a spectral resolution within ± 1 cm^{-1}.

For all the samples, the analyses were conducted in different spots of the surface, keeping the power of the laser at a maximum value of 0.25 mW to avoid the induction of different phases and/or the carbonization of the samples.

2.4. Stiction propensity measurements

The stiction tendency of the different friction materials produced in this study was evaluated through the stiction test, an electrochemical methodology patented by ITT Inc. This procedure, previously described in detail in other studies [7,40], employs a purpose-designed electrochemical cell developed to induce and analyze the stiction phenomenon under controlled laboratory conditions. Briefly, the cell is based on a three-electrode configuration and is equipped with a clamping system (screw) that is used to keep the gray cast iron sample in contact with a friction material sample. A cast iron cylinder with a 1 cm diameter embedded in epoxy resin was used as a working electrode. An electric contact was made on the back of the gray cast iron sample in order to provide an electrical connection to the potentiostat. To simulate the real grit of a braking disc, the WE surface was ground with silicon carbide grinding papers with 220 grit. An Ag/AgCl (KCl 3 M) electrode and a graphite bar were employed as the reference and counter electrodes, respectively. Samples of friction materials produced by ITT Inc. with a 10 mm diameter were used for stiction tests.

Although the exact composition of the friction materials used in this study is proprietary, all formulated materials belong to the Non-Asbestos Organic (NAO) category. These complex formulations contain 5–15%$_V$ of solid lubricants such as MoS_2 and graphite, 5–15%$_V$ of abrasives including Al_2O_3, ZrO_2, and chromite, 5–20%$_V$ of fillers like barite and vermiculite, and 5–20%$_V$ of fibers. The term "organic" reflects the primary use of aramid and glass fibers, whereas steel fibers are strictly limited to concentrations below 15%$_W$.

A pad holder was employed to ensure the contact between the pad and the gray cast iron sample. A disc surface area slightly greater than that of the friction material (1.5 cm diameter) was exposed to the electrolyte, enabling the investigation of corrosion phenomena at the interface between the two materials. A schematic representation of the set-up is reported in Fig. 1.

A clamping system consisting of a screw and a bar was employed to ensure a constant clamping force during stiction tests. This setup simulates the static contact between the brake disc and friction material that is responsible for stiction in automotive braking systems.

The cast iron WE, coupled with the friction material, was subsequently immersed in the electrolyte solution in order to promote stiction, inducing the corrosion of the cast iron sample by means of potentiodynamic polarization. For this experimental procedure, we deliberately decided to employ a 0.1 M NaCl solution instead of a 0.1 M HCl solution because the testing configuration with the gray cast iron in contact with the friction material samples promotes the formation of an occluded cell, and there is no need to simulate an acidic environment.

The use of this electrolyte makes it possible to perform the stiction procedure under testing conditions similar to those occurring in vehicles during service, preserving at the same time the same chloride concentration used in the electrochemical analyses.

After stiction induction, the tangential force to separate the friction material sample from the disc sample was measured by means of a bench dynamometer (Fig. 2). This force is referred to as the “stiction force” in this work. The measurement of the stiction force provided a quantitative method to evaluate the susceptibility to stiction of the friction material. The surfaces of the gray cast iron disc and friction material samples were also inspected by means of an optical stereo-microscope (ZEISS SteREO Discovery.V12) after the measurements of the stiction force to evaluate the damage of the friction material and its adhesion on the disc samples. In order to assess the reproducibility of the results, at least 6 measures were repeated for each sample. A non-commercial friction material exhibiting a high susceptibility to the stiction phenomenon was employed as the blank sample. Subsequently, a series of stiction tests was conducted using electrolyte solutions containing the selected inhibitors. For sodium oxalate, the same concentration of 0.02 M adopted for the electrochemical characterization of the inhibition mechanism was employed, whereas 2,5-PDA was used at saturation due to its lower solubility in neutral solutions (nominal water solubility at room temperature is approximately 1.237 g/L). In selecting the concentrations, we must consider that the pad-disc interface is a highly confined and transient environment, in which crevice corrosion leads to progressive acidification at the interface. For a molecule like 2,5-PDA, this local drop in pH induces protonation, which can significantly increase its local solubility compared to the neutral bulk solution. Therefore, the actual concentration of active inhibitor at the disc-friction material interface is dynamic and heavily influenced by local chemical gradients. Since quantifying the exact instantaneous concentration at the hidden interface *in operando* is virtually impossible, a saturated solution of 2.5-PDA (the less soluble specie) was selected to evaluate its maximum potential efficacy as a solution-based inhibitor. For sodium oxalate (the more soluble specie), we used a higher concentration (0.02 M) because its superior solubility easily allows more inhibitor to reach the interface from the external environment.

Relying on an external solution-based inhibitor leads to a complex protection mechanism; therefore, a secondary approach based on the incorporation of the inhibitor directly into the friction material formulation was used as the most effective strategy to guarantee its presence at the interface exactly where and when corrosion starts, regardless of bulk solubility limits.

For this purpose, ITT Inc. selected sodium oxalate as an additive to modify the composition of a blank friction material due to its high

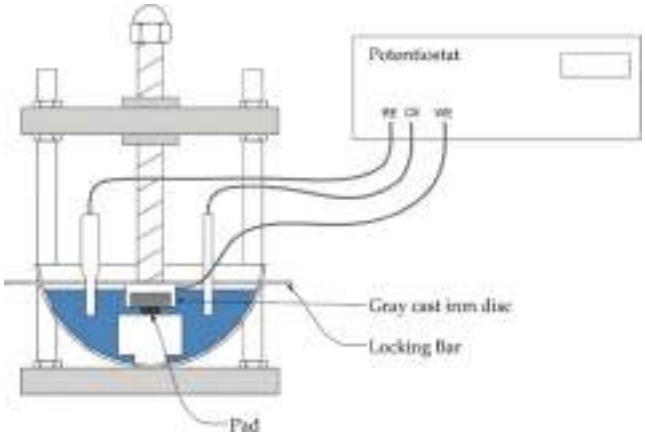

Fig. 1. Set-up adopted for the stiction test.

Fig. 2. Bench dynamometer for stiction force measurements.

solubility and lower price compared to 2,5-PDA. The blank material was a non-commercial friction material with a known high susceptibility to stiction.

Stiction tests for friction materials containing 4%$_w$ and 6%$_w$ of sodium oxalate were carried out according to the procedure described above. Specifically, the stiction tests adopted in this study investigate the short-term performance of friction materials. This was motivated by the fact that typical conditions for stiction include the activation of the parking brake with a new friction material, such as during oversea transfer of vehicles after the production.

3. Results and discussion

3.1. Time-dependent potentiodynamic polarization

Fig. 3 shows the time-dependent potentiodynamic polarization curves after 10 min (Fig. 3**A**), 6 h (Fig. 3**B**), and 24 h of immersion (Fig. 3**C**) with and without 2,5-PDA in the 0.1 M HCl solution. As shown in Fig. 3**A**, 2,5-PDA already exhibits inhibitory effects after only 10 min of immersion. Furthermore, the minimal shift in corrosion potential, together with the reduction in cathodic and anodic current densities, suggests a mixed-type inhibition mechanism. No significant changes in the shape of the polarization curves are observed in the anodic and cathodic Tafel regions when comparing the systems with and without 2,5-PDA. This behavior indicates that, after 10 min of immersion, the inhibitive effect is likely associated with the adsorption of the inhibitor onto the gray cast iron surface, showing a 49% inhibition efficiency based on Tafel analysis (Table 2).

Potentiodynamic polarization measurements were subsequently repeated after 6 h of immersion (Fig. 3**B**). A marked increase in corrosion current density is observed for the uninhibited solution, whereas the system containing the inhibitor exhibits relatively stable behavior (Table 2). In particular, in the presence of 2,5-PDA, no significant variation in cathodic current density is detected between 10 min and 6 h of immersion. Furthermore, the anodic branch reveals the emergence of a pseudo-passive behavior which is likely associated with a secondary inhibition mechanism involving the formation of a precipitated protective layer [8]. The pseudo-Tafel analysis adopted to calculate the inhibition efficiency, shows an increased inhibition efficiency of 64% after 6 h of immersion. The stability of this pseudo-passive layer was then assessed by performing potentiodynamic polarization measurements after 24 h of immersion. The results based on pseudo-Tafel analysis are reported in Table 2, showing an increase in corrosion current density for the sample in the solution without the inhibitor increasing the immersion time from 10 min to 6 h and then 24 h. Conversely, in the presence of 2,5-PDA, the protective layer formed after 6 h of immersion keeps the sample protected, showing even a slight decrease of corrosion current density from 6 to 24 h of immersion (Table 2).

The same measurements were repeated using the acidic electrolyte solution containing sodium oxalate. The potentiodynamic polarization curves obtained after 10 min of immersion (Fig. 4**A**) display a reduction of both the anodic and the cathodic current densities in the solution containing sodium oxalate relative to the blank solution. This suggests that, for a low immersion time, sodium oxalate acts as a mixed inhibitor for gray cast iron. Nevertheless, the presence of a predominant anodic behaviour becomes clear for longer immersion times of 6 h and 24 h, at which the reduction of the anodic currents and the shift of the corrosion potentials, 52 and 50 mV respectively, are rather marked. A pseudo-passive range is also visible for the curves recorded after 6 and 24 h of immersion.

Data in Table 2 clearly highlight that, similarly to 2,5-PDA, the inhibitor efficiency increases with the immersion time, with a remarkable efficiency of 91% for the polarization curves acquired after 24 h of immersion.

A plausible explanation for the differences concerning the anodic and cathodic behaviour of 2,5-PDA and sodium oxalate may reside in the different chemical structure of the two inhibitors. As reported in our previous work concerning 8-HQ [8], the aromatic and pyridinic structure of 2,5-PDA may favour a stronger adsorption on the gray cast iron disc. This adsorption may lead to the formation of an ordered template on the surface of the gray cast iron disc, over which the growth of the 2,5-PDA-Fe complex can evolve in a homogeneous and ordered way, providing the formation of a compacted structure.

A similar mechanism can also be proposed for sodium oxalate, although with some differences. The higher inhibition efficiency observed after 10 min suggests faster adsorption, likely due to lower steric hindrance. However, this adsorption appears to promote the formation of a different surface structure that mainly hinders the anodic reaction, without significantly affecting the cathodic proton reduction. Overall, time-dependent potentiodynamic polarization measurements suggest a slightly higher inhibition efficiency for sodium oxalate compared to 2,5-PDA over the times of immersion studied in this work.

3.2. Electrochemical impedance spectroscopy

Electrochemical impedance measurements were further employed to characterize the formation and long-term stability of the 2,5-PDA and sodium oxalate protective films.

Fig. 5 shows the main results obtained in the form of Bode plots up to 15 days of immersion in the electrolyte solution containing 2,5-PDA (Fig. 5**A**) and sodium oxalate (Fig. 5**B**). The spectra obtained can be rationalized by considering, in both cases, the kinetics of the different processes involved in the formation and evolution of the protective layer. In the presence of 2,5-PDA in the acidic electrolyte solution, a slight increase in the impedance module at low frequency is consistently

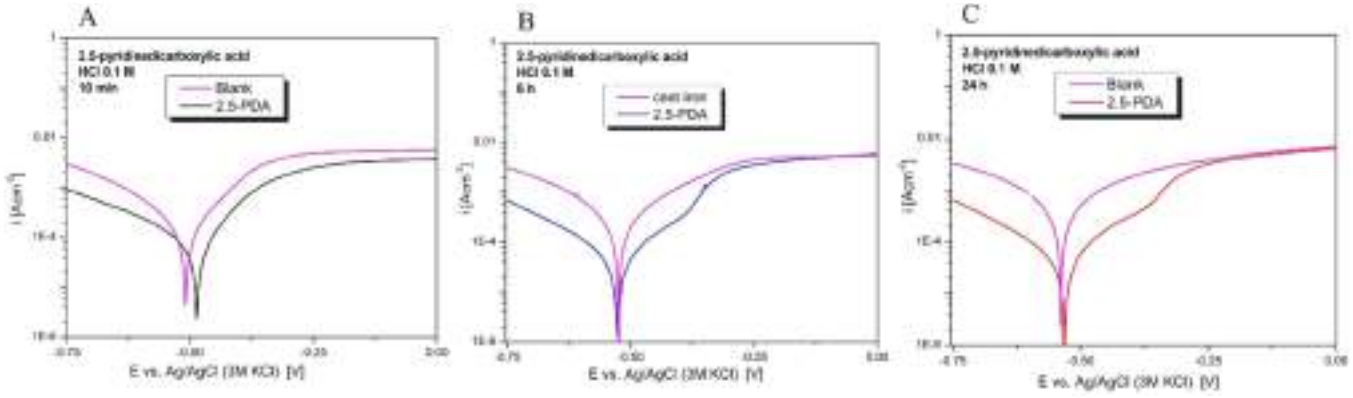

Fig. 3. Time-dependent potentiodynamic polarization curves of gray cast iron in the blank solution vs. the acidic solution containing 2,5-PDA after 10 min (A), 6 h (B), and 24 h of immersion (C).

Table 2
Corrosion potentials (E_{corr}), corrosion current densities (i_{corr}), and inhibition efficiencies values (η) obtained from the time-dependent potentiodynamic polarization measurements. The σ values are the standard deviations of each parameter for the three experiments conducted for each analysis.

Electrolyte	Concentration [mol·l^{-1}]	Time	E_{corr} [mV]	σ_E_{corr} [mV]	i_{corr} [mAcm^{-2}]	σ_i_{corr} [mAcm^{-2}]	η [%]	σ_η [%]
HCl 0.1 M	-	10 min	−514	5	0.094	0.009	-	-
		6 h	−522	2	0.139	0.036		
		24 h	−534	10	0.300	0.028		
HCl 0.1 M	0.02	10 min	−492	6	0.048	0.001	49	2
+		6 h	−524	1	0.050	0.022	64	16
2,5-PDA		24 h	−559	10	0.041	0.015	87	5
HCl 0.1 M	0.02	10 min	−492	6	0.044	0.004	54	5
+		6 h	−470	6	0.023	0.012	84	8
Sodium Oxalate		24 h	−484	8	0.027	0.001	91	1

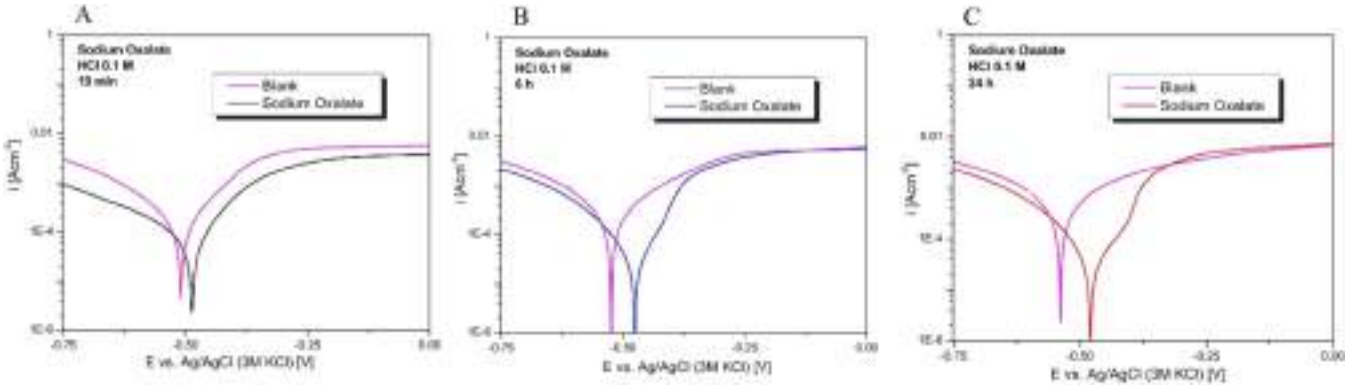

Fig. 4. Time-dependent potentiodynamic polarization curves of gray cast iron in the blank solution vs. the acidic solution containing sodium oxalate ($Na_2C_2O_4$) after 10 min (A), 6 h (B), and 24 h of immersion (C).

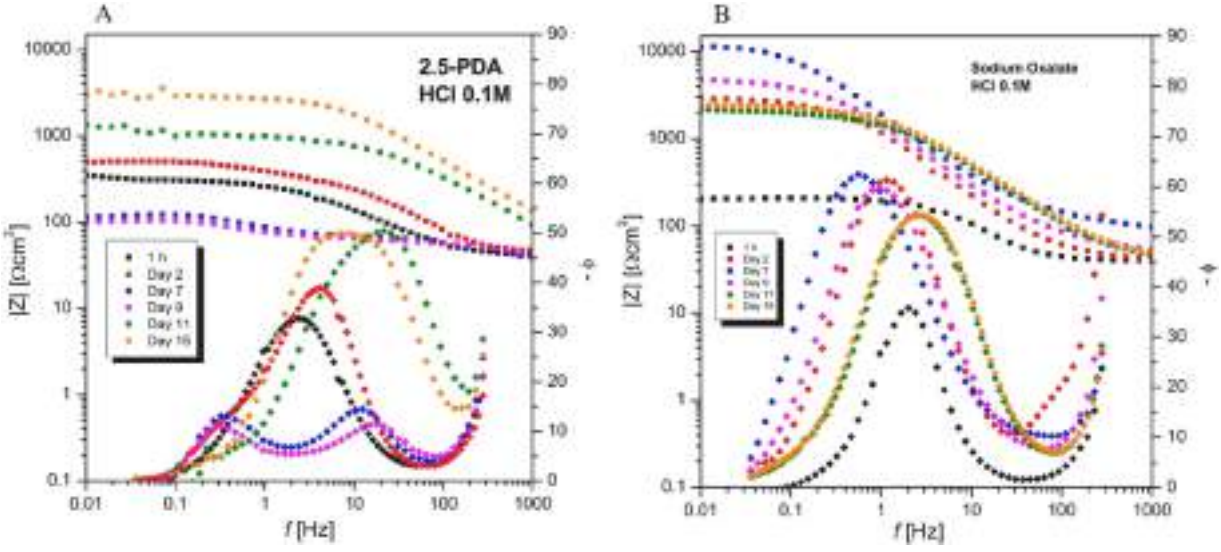

Fig. 5. Impedance measurements up to 15 days of immersion of gray cast iron samples in the electrolyte solution containing 0.02 M of 2,5-PDA (A) and sodium oxalate (B).

observed after 1–2 days of immersion. In agreement with the presented PDP curves, this behavior may be attributed to the formation of an adsorbed 2,5-PDA layer, occurring in competition with other surface processes, such as the rearrangement of the adsorbed species on the gray cast iron disc and the dissolution of iron into ionic form. The latter process is predominant during the early stages of immersion, resulting in a steady decrease in the low-frequency impedance modulus. Indeed, a progressive decrease in the corrosion resistance of the sample can be observed over the subsequent seven days of immersion. In addition, the appearance of two distinct time constants can be identified, associated with the response of the gray cast iron substrate and that of a mixed layer composed of inhibitor species and corrosion products. These features are accompanied by lower phase angle values in absolute values, indicative of the increasing complexity of the interfacial processes. For immersion times longer than 9 days, a progressive increase in the impedance module at low frequency is observed, accompanied by a continuous increase in the phase angle in absolute value. Additionally, the impedance spectrum evolves toward a profile characteristic of the formation of

a compact and more protective surface layer (Fig. 5**A**). Additionally, the reduction in electrolyte conductivity, particularly evident after 15 days of immersion, may indicate that iron ions participate in the formation of this protective layer.

The same measurements were performed in the presence of sodium oxalate (Fig. 5**B**). As observed in the previous system, an increase in the impedance module at low frequency is detected after 1–2 days of immersion. However, the values of the impedance module are consistently higher than those obtained in the presence of 2,5-PDA. In agreement with the polarization results, this behavior suggests a more homogeneous surface coverage and faster adsorption kinetics of sodium oxalate on the gray cast iron substrate compared to 2,5-PDA.

Following this initial stage, a further increase in the low-frequency impedance modulus is observed after 9 days of immersion. This increase is accompanied by an increase in the phase angle absolute value and a reduction in the electrolyte conductivity, as evidenced by the Bode spectra reported in Fig. 5**B**. Similarly to results obtained for 2,5-PDA, the simultaneous increase in impedance modulus and electrolyte resistance may indicate the formation of a surface precipitate layer. This phenomenon can be attributed to the interaction between dissolved iron ions and oxalate species, leading to the formation of insoluble complexes that deposit on the surface. Such precipitation effectively reduces the concentration of free iron ions in the electrolyte and contributes to the development of a protective layer on the gray cast iron surface.

Despite the higher values of the impedance module at low frequency and the higher phase angle in absolute value for the same time (7 days) with respect to 2,5-PDA, the precipitated protective layer can be inferred to be less stable than that formed in the presence of 2,5-PDA considering the trend of the spectra at longer immersion times. Indeed, while a continuous increase in the low-frequency impedance modulus is visible in the electrolyte containing 2,5-PDA up to 15 days of immersion, the opposite trend is found for the solution containing sodium oxalate. In the latter case, the impedance module does not show a sustained increase over time, suggesting that the protective layer formed by oxalate species is less stable and may undergo partial dissolution or restructuring during prolonged exposure. Nevertheless, it is possible to claim that both the inhibitors are effective in reducing the corrosion of the gray cast iron disc for a prolonged time of immersion.

Contrary to the polarization analysis, impedance measurements were not used to determine the inhibition efficiencies of 2,5-PDA and sodium oxalate. This decision was based on the observation that, although the samples exhibited similar qualitative behavior, the formation of the adsorbed layer responsible for the protective film occurred at slightly different immersion times for different samples. Consequently, the impedance module at low frequency were quite different for the different times of immersion, making it difficult to obtain a precise value for the inhibition efficiencies. A plausible explanation for this variability may reside in the stochastic nature of the inhibitive processes under investigation. Indeed, following the initial adsorption of the inhibitor on the surface of the gray cast iron disc, an important prerequisite for the formation of a protective precipitated layer is the attainment of the concentration of saturation for the precipitating species. This process depends on the buildup of a sufficient concentration of dissolved iron ions, which is intrinsically linked to the early-stage corrosion behavior of the substrate, as well as to the adsorption dynamics of the inhibitor at the metal–solution interface. Consequently, despite similar qualitative behavior, fluctuations in these processes may lead to significant variability in terms of the quantitative response of the impedance spectra.

These considerations do not apply to the polarization measurements previously discussed. Indeed, while impedance measurements study the evolution of the system as a function of immersion time under open circuit potential conditions, polarization analysis reflects an instantaneous state of the system under an externally applied perturbation. In particular, anodic polarization measurements force the system toward the production of iron ions, promoting the formation of the precipitated protective layer at the metal–solution interface. As a result, the polarization response is less influenced by the stochastic temporal evolution observed under open circuit conditions.

Despite this consideration, by comparing the measured values with those reported in the literature for gray cast iron in the same electrolyte in the absence of inhibitors [8,10], it can be easily inferred that both 2,5-PDA and sodium oxalate exhibit inhibitive properties towards the corrosion of the gray cast iron disc.

3.3. Optical and FE-SEM/EDX characterization

Optical observation and composition analysis were further conducted to confirm the interpretation suggested from the electrochemical measurements. Fig. 6 shows the condition of the gray cast iron disc surface following the impedance measurements at 7 days (Fig. 6**A**) and 15 days of immersion (Fig. 6**B**). Fig. 6**A** seems to suggest that precipitation over the surface of the gray cast iron disc starts even before 7 days of immersion in the presence of 2,5-PDA. Nevertheless, as the magnified image of the surface shows, the formation of a crystalline precipitate layer is still incomplete, and red scarlet crystalline precipitates are separated by yellowish zones in which corrosion products are still visible.

Fig. 6**B** shows the surface of the gray cast iron disc after the 15 days impedance measurements. As correctly suggested from the impedance spectra, the surface appears to be completely covered with the red scarlet crystalline product that was only partially covering the surface for a shorter time of immersion.

Fig. 7 presents the qualitative EDX analysis of the red scarlet protective layer. The EDX elemental maps indicate that the primary elements constituting the layer are carbon, oxygen, and iron. In addition, nitrogen is detected and appears to be relatively homogeneously distributed throughout the layer.

The average thickness of the protective layer is approximately 100 μm based on cross-section measurements. Nevertheless, spatial variations in thickness are also observed; specifically, the area with no signals reported in Fig. 7 in the maps of the individual elements can be associated with a local thickness discontinuity of the protective film.

Table 3 summarizes the semi-quantitative chemical composition obtained by EDX analysis of the area shown in Fig. 7. The elevated concentrations of nitrogen and carbon provide clear evidence of the presence of 2,5-PDA on the surface of the gray cast iron sample. Moreover, the corresponding carbon and nitrogen signals overlap with those of iron and oxygen in the entire crystalline layer. These observations support the hypothesis of the formation of a precipitated complex involving 2,5-PDA and iron ions.

The same analysis was further conducted for the disc with the solution containing sodium oxalate. Fig. 8 illustrates the surface condition of the gray cast iron disc after 15 days of immersion following the electrochemical impedance spectroscopy measurements. The formation of a yellowish crystalline layer is clearly evident on the sample surface following immersion in the acidic solution containing sodium oxalate (Fig. 8**A**).

In contrast to the results obtained with 2,5-PDA, the protective layer in the presence of sodium oxalate was already clearly detected and verified by its electrochemical barrier properties after 7 days of immersion (Fig. 5**B**); therefore, Fig. 8 only reports the gray cast iron disc surface after 15 days of immersion. A higher-magnification image obtained by FE-SEM is reported in Fig. 8**B**. In analogy with the system containing 2,5-PDA, sodium oxalate appears to promote the formation of a crystalline layer on the surface of the gray cast iron disc. However, in this case the crystals of the deposit exhibit a significantly different structure compared to that observed in the presence of 2,5-PDA.

EDX qualitative elemental maps acquired on a crystalline spot of the surface film is reported in Fig. 9. The presence of a homogeneous distribution of iron, carbon, and oxygen, as reported in the maps of the singular element (Fig. 9**B-D)**, can explain the effect of sodium oxalate on the anodic current densities in terms of the formation of an insoluble

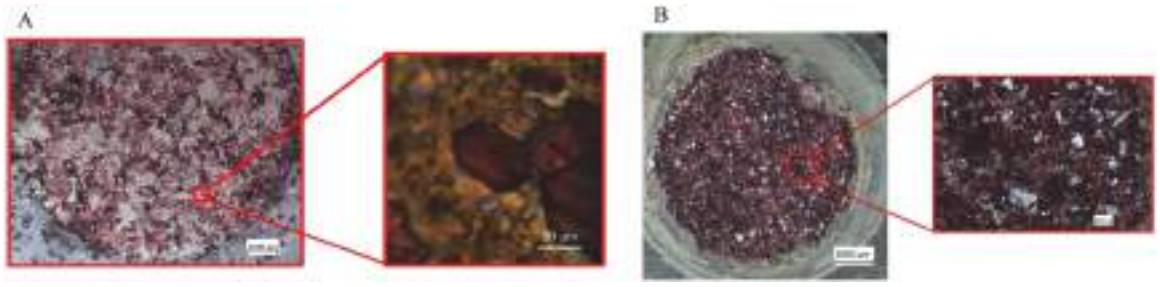

Fig. 6. Stereomicroscope image of a gray cast iron disc sample immersed in a 0.1 M HCl solution 0.02 M of 2,5-PDA for 7 days (A) and 15 days of immersion (B).

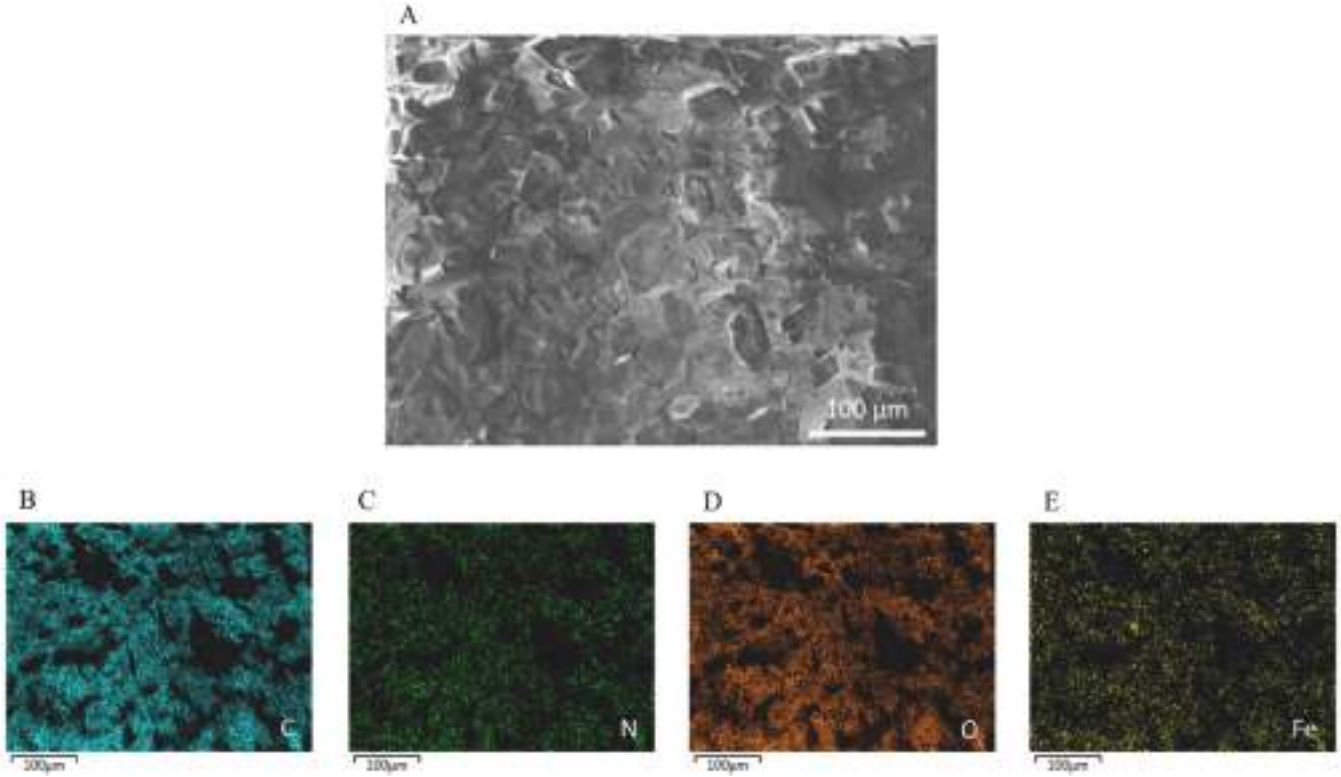

Fig. 7. FE-SEM secondary electron image of the crystalline complex formed after 15 days of immersion of a gray cast iron sample in a 0.1 M HCl solution 0.02 M of 2,5-PDA (A), EDX elemental maps of the single elements captured from the surface (B for carbon, C for nitrogen, D for the oxygen, and E for iron).

Table 3
Semi-quantitative results obtained from area-integrated EDX analysis.

Inhibitor	Element	$\%_w$	σ
2,5-PDA	Fe	42	0.2
	O	32	0.1
	C	23	0.1
	N	3	0.1
Sodium oxalate	O	49	0.4
	Fe	38	0.5
	C	13	0.2

complex between oxalate ions and ferrous ions. In this regard, the chemical composition of a FeC_2O_4 complex, with a weight percentage of 39% Fe, 17% C, and 44% O strongly resembles the atomic weight percentage obtained from the semiquantitative analysis reported in Table 3. This suggests that the immersion in the 0.1 M HCl solution containing 0.02 M of sodium oxalate leads to the formation of a protective layer of FeC_2O_4.

3.4. Raman characterization

To confirm the proposed hypothesis, Raman spectroscopy measurements were further conducted, comparing the protective layers with the Raman spectra of the respective inhibitors in powder. The results are reported in Fig. 10. Raman analyses were conducted on the different areas of the gray cast iron disc samples after 7 days of immersion for 2,5-PDA and 15 days of immersion of sodium oxalate. In this last case, measurements at 7 days were not considered because of the fastest formation of the protective layer on the surface of the gray cast iron disc.

From the analysis reported in Fig. 10**A,** it is possible to claim with certainty the involvement of the inhibitor in the yellowish area (Fig. 6**A**), as well as in the red scarlet one (Fig. 6**A**). In this first case, the appearance of new peaks at 732 and 1144 cm^{-1} could be connected with the direct interaction between the organic molecule and the gray cast iron corrosion products in the proximity of the substrate. Specifically, the presence of these peaks may be tentatively assigned to ring deformation modes in proximity to the metal surface and to the initial coupling with iron ions, predominantly constituted of Fe^{2+} ions generated by the initial anodic dissolution of cast iron in the acidic solution.

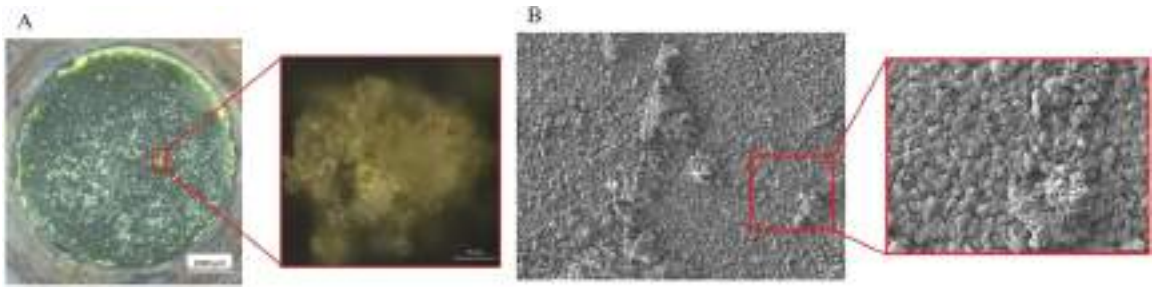

Fig. 8. Stereomicroscope image of a gray cast iron disc sample immersed for 15 days in a 0.1 M HCl solution 0.02 M of sodium oxalate (A), FE-SEM magnified image of the crystalline deposit on the surface of the gray cast iron disc (B).

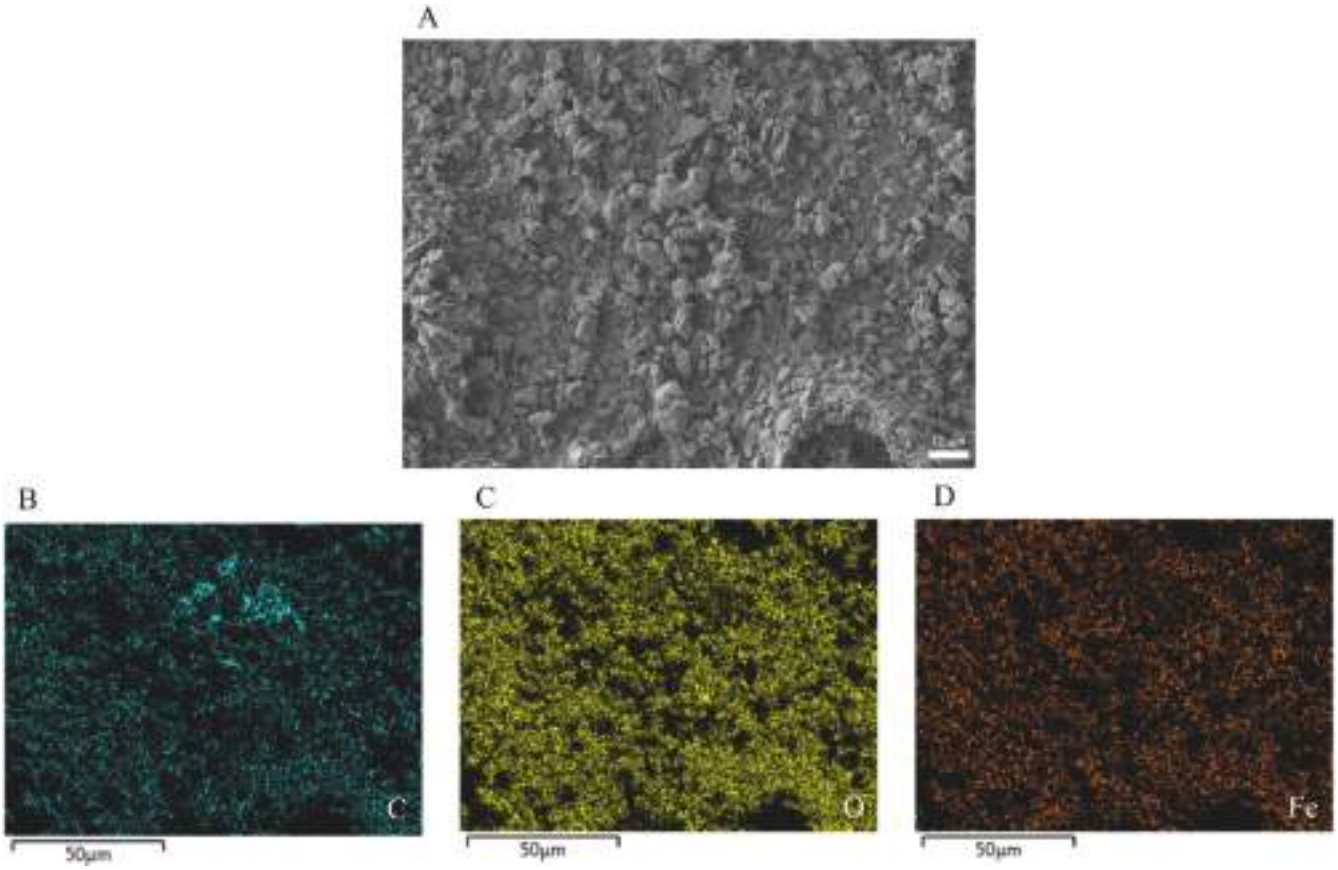

Fig. 9. FE-SEM secondary electron image of the crystalline complex formed after 15 days of immersion of a gray cast iron sample in a 0.1 M HCl solution 0.02 M of sodium oxalate (A), EDX elemental maps of the single element captured from the surface (B for carbon, C for oxygen, D for iron).

Conversely, a more structured spectra can be seen in the red scarlet areas (red spectra in Fig. 10**A**). A major indicator of this chemical transition is the marked shift of the main peaks of the 2,5-PDA powder and their sharpening compared to the spectra in yellow areas. The transition from the yellowish to the reddish morphology is consistent with the oxidation of Fe^{2+} to Fe^{3+}.

The same analyses were conducted on the protective layer formed on the gray cast iron disc in the solution containing sodium oxalate after 15 days of immersion. In this case, in agreement with the EDX analysis, the Raman spectra of the protective layer in Fig. 10**B** can be confidently assigned to iron (II) oxalate dihydrate. Specifically, the prominent and sharp peak observed at 1467 cm^{-1} can be assigned to the very strong CO stretching mode reported for solid iron (II) oxalate [41]. Similarly, the peak at 912 cm^{-1} matches the vibration mode of the CO\CC coupled identified in the literature [41]. Besides, the absence of multiple high-frequency bands in the 1600–1700 cm^{-1} region is a sign that the significant presence of iron (III) oxalate species can be excluded, confirming that the interaction between the sodium oxalate solution and the cast iron substrate yields a well-defined, crystalline iron (II) oxalate passivating film [41].

3.5. Stiction test measurements

A non-commercial friction material (blank), strongly susceptible to the stiction phenomenon, was selected in order to assess the effect of 2,5-PDA and sodium oxalate on the stiction phenomenon. Stiction tests were first conducted on this material in a 0.1 M NaCl solution and compared with stiction tests performed with the inhibitors added in the electrolyte solution. Table 4 reports the average value of the stiction force and the standard deviation obtained based on six different measurements.

The average stiction force is 92 N for stiction tests performed in 0.1 M NaCl solution, confirming the very high susceptibility of the blank

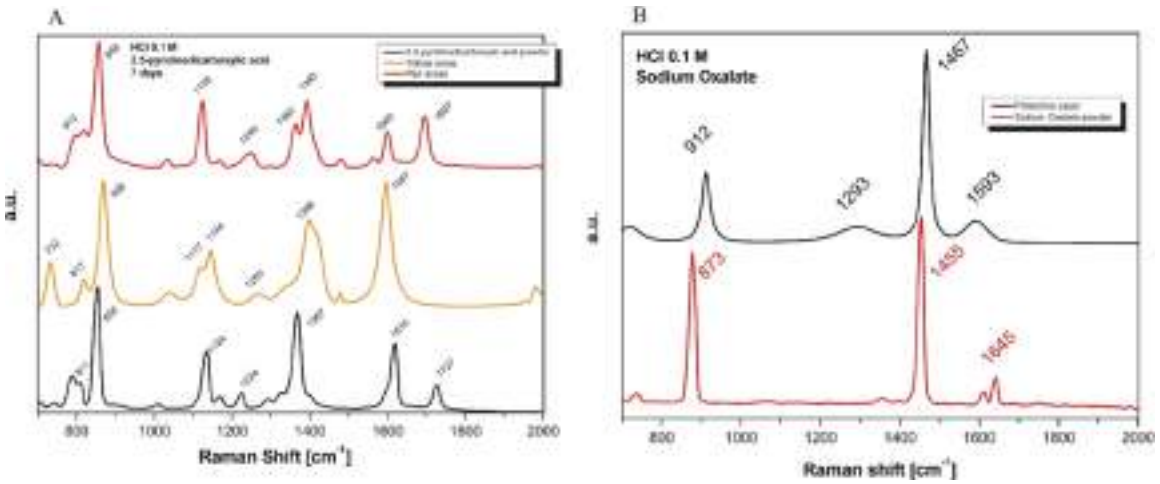

Fig. 10. Raman spectra of 2,5-PDA powder in comparison with the spectra of the yellowish and the red areas highlighted in Fig. 6 (A); Raman spectra of sodium oxalate powder and of the protective layer highlighted in Fig. 8 (B).

Table 4
Average stiction forces obtained after the induction of the stiction phenomenon (F_s) with the relative standard deviations (σ_F_s) for stiction test conducted with the inhibitor in the electrolyte solution.

Friction Material	Electrolyte solution	F_s [N]	σ_F_s [N]
Blank	NaCl 0.1 M	92	15
	NaCl 0.1 M + 2,5-PDA saturation	24	8
	NaCl 0.1 M + Sodium Oxalate 0.02 M	19	9

friction material employed in this work.

After stiction and detachment from the friction material sample, the surface of the rotor sample exhibits abundant corrosion products and portions of friction material sticking on the rotor surface (Fig. 11**A**). In particular, the adhesion of the friction material is marked at the periphery of the contact region with the friction material due to the specific assembly of the samples that strongly favours crevice corrosion in this region. The friction material sample exhibits severe damage after stiction with some portions of material removed during the detachment from the rotor (Fig. 11**B**). These correspond to the residuals of friction material that are visible on the rotor sample (Fig. 11**A**). Moreover, red corrosion products are visible also on the surface of the friction material, as a result of the strong corrosion of the gray cast iron during the stiction test. The morphology of the rotor and friction material after the stiction test indicates that a high stiction force is associated with severe damage of the friction material.

The same test performed in 0.1 M NaCl solution was repeated in the same electrolyte containing 2,5-PDA at saturation and 0.02 M sodium oxalate. Fig. 12 reports the stiction force measured in the presence of the inhibitors. Fig. 12**A** and Fig. 12**C** display the morphology of the rotor samples, and Fig. 12**B** and **D** that of the friction material samples after detachment. The stiction forces are 24 and 19 N, respectively, for the stiction tests carried out in the solution containing 2,5-PDA at saturation and 0.02 M sodium oxalate, which are significantly lower than those measured in the solution without inhibitors. This indicates that the high susceptibility to stiction of the friction material is strongly reduced by the addition of complexing inhibitors in the testing electrolyte. This is associated with a very limited amount of friction material transferred on the rotor surfaces (Fig. 12**A** and **C**) and very low damage of the friction materials (Fig. 12**B** and **D**). These preliminary results indicate that the introduction of the inhibitor in the friction material could effectively reduce its susceptibility to stiction phenomena, even for the highly susceptible friction material that was deliberately selected for this work.

Finally, sodium oxalate was selected in order to investigate the direct addition into the blank friction material. Blank friction materials containing 4 and 6%$_w$ sodium oxalate in place of barium sulfate were produced. Considering the concentrations explored in this study, this substitution was kept at a minimal percentage relative to the substantial total amount of barium sulfate in the blank mix. Given this minor fraction, the replacement does not significantly alter the hydrophobicity, thermal stability, or mechanical properties of the pad. Therefore, sodium oxalate does not compromise the properties of the friction material, acting solely as active inhibitor. Consequently, stiction tests were

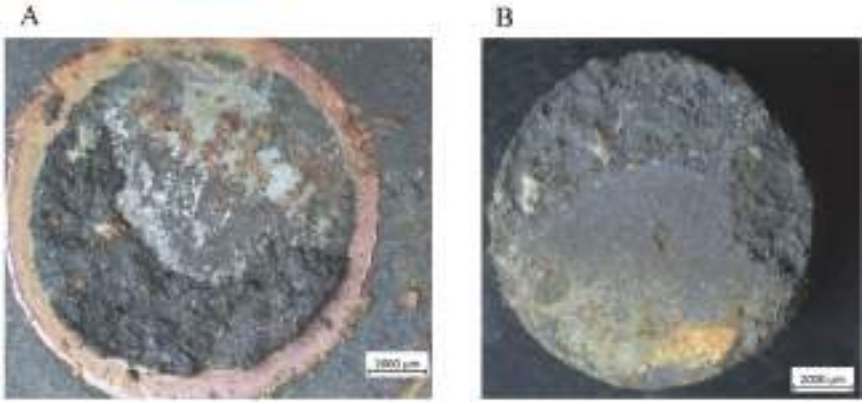

Fig. 11. Gray cast iron disc (A) and blank friction material samples after the stiction measurements (B).

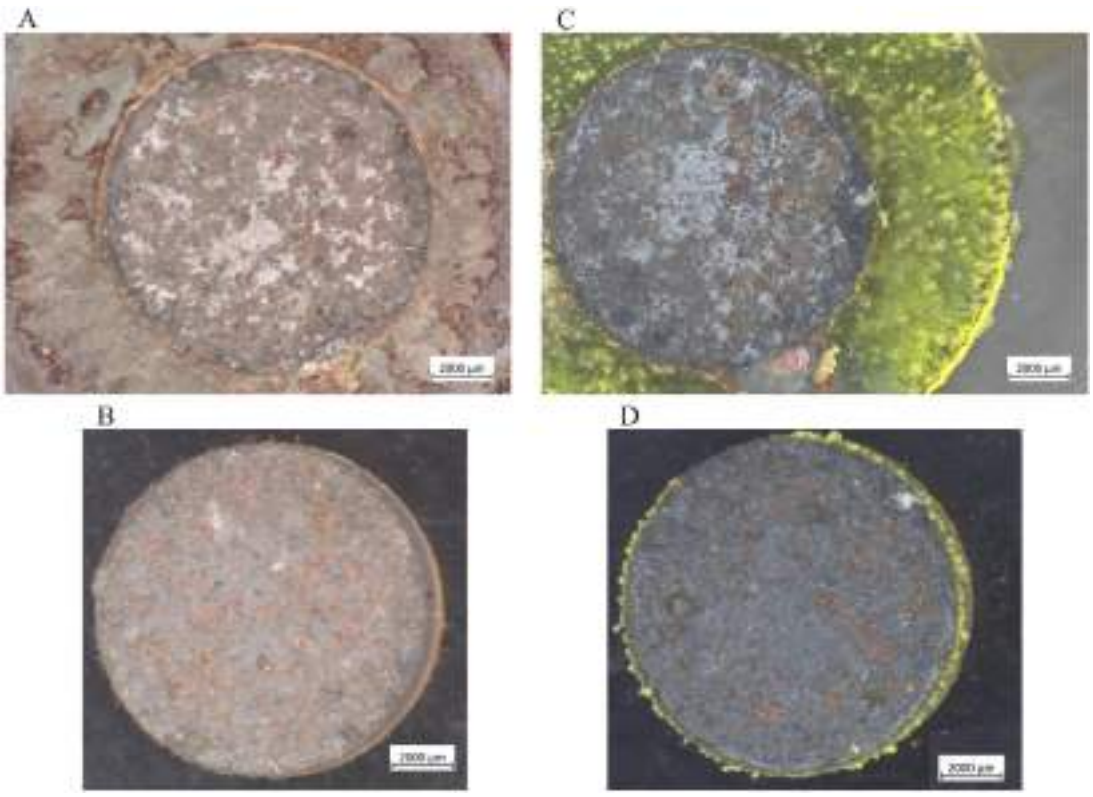

Fig. 12. Stereomicroscope image of the gray cast iron disc that was in contact with the blank friction material in the 0.1 M NaCl 2,5-PDA saturated solution post detachment (A), Stereomicroscope image of the blank friction material that was in contact with the gray cast iron disc in the 0.1 M NaCl solution 2,5-PDA saturated solution post detachment (B), Stereomicroscope image of the gray cast iron disc that was in contact with the blank friction material in the 0.1 M NaCl 0.02 M sodium oxalate solution post detachment (C), Stereomicroscope image of the blank friction material that was in contact with the gray cast iron disc in the 0.1 M NaCl solution 0.02 M sodium oxalate solution post detachment (D).

conducted on these materials in a 0.1 M NaCl electrolyte solution free of inhibitors (Table 5).

The average stiction force of the friction materials containing sodium oxalate is 28 N for the friction material with 4% of sodium oxalate and 11 N for that with 6% of sodium oxalate. This is significantly lower than the value obtained for the reference friction material (Table 5). The stiction test protocol utilized at the University of Udine is strictly correlated and validated with vehicle field tests. In automotive applications, a residual force below 20 N is universally considered a "stiction-free" condition, as it does not cause any perceptible brake damage, noise, or operational issues upon vehicle restart.

With reference to the stiction tests carried out in this work, it is possible to conclude that sodium oxalate is a viable inhibitor for the control of the stiction phenomenon in automotive braking systems. Besides, an increase of the content of sodium oxalate in the friction formulation (from 4% to 6% by weight) results in a further reduction of the stiction force. Fig. 13 reports the images of the discs and friction materials following the stiction force measurements.

No visible traces of the green/yellow **FeC_2O_4** complex can be visibly detected in the case of the sodium oxalate inhibitor directly added to the friction material. However, no evidence of corrosion or fragments of friction material can be identified on the surface of the grey cast iron samples. The scratching of the sample surface due to grinding is still evident after the stiction test; besides, no significant damage to the 4%-Sodium Oxalate and the 6%-Sodium Oxalate friction material samples can be detected after the stiction test. Although FeC_2O_4 complexes were not detected directly on the disc surface, this does not rule out the chemical inhibition mechanism discussed above for sodium oxalate. Commercial friction materials are highly complex multi-component systems that contain, among other ingredients, steel fibres. It is highly probable that the sodium oxalate reacts locally with the iron fibres inside the porous matrix of the pad. This reaction likely forms a localized complex that acts as a "plugging" agent (similarly to the mechanism documented for zinc additives in friction materials [7]), sealing the surface pores of the pad and physically blocking the penetration of external disc corrosion products. Due to the vast number of constituents in commercial formulations, isolating this intra-porous phase directly is inherently difficult; therefore, confirming its precise nature would require dedicated studies on simplified model materials.

Table 5
Average stiction forces obtained after the induction of the stiction phenomenon (F_s) with the relative standard deviations (σ_F_s) for stiction test conducted with sodium oxalate as additive in the blank friction material.

Friction Material	Electrolyte solution	F_s [N]	σ_F_s [N]
Blank	NaCl 0.1 M	92	15
$4\%_w$ Sodium Oxalate	NaCl 0.1 M	28	8
$6\%_w$ Sodium Oxalate	NaCl 0.1 M	11	3

4. Conclusions

This work investigated the inhibitive properties of complex-forming organic corrosion inhibitors and their effect on the stiction phenomenon in automotive braking systems. Specifically, the beneficial effects of 2,5-PDA and sodium oxalate on cast iron corrosion. From this study, we can finally conclude that:

- PDP analyses revealed that 2,5-PDA exerts a mixed inhibitory action, forming a pseudo-passive layer after 6 h. A similar mechanism was observed for sodium oxalate; however, its lower steric hindrance

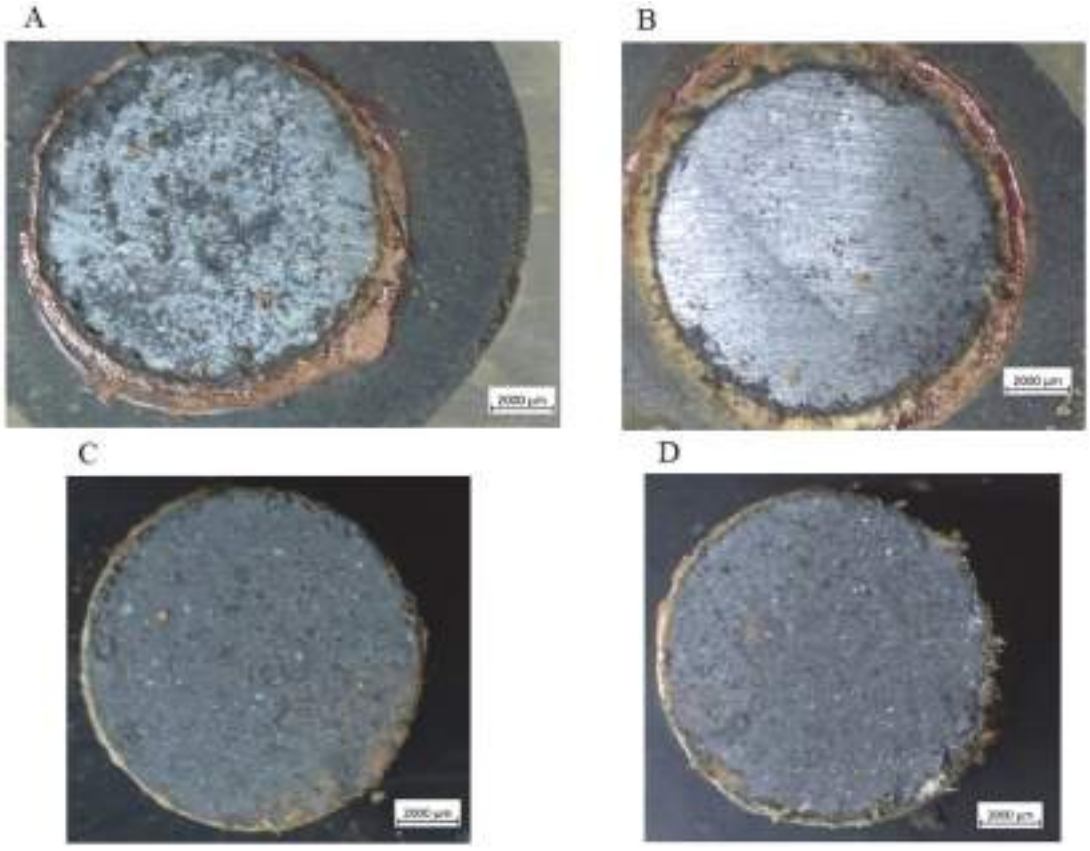

Fig. 13. Stereomicroscope image of the gray cast iron disc that was in contact with the 4%$_w$-Sodium Oxalate friction material in the 0.1 M NaCl solution post detachment (A), Stereomicroscope image of the gray cast iron disc that was in contact with the 6%$_w$-Sodium Oxalate friction material in the 0.1 M NaCl solution post detachment (B), Stereomicroscope image of the 4%$_w$-Sodium Oxalate friction material that was in contact with the gray cast iron disc in the 0.1 M NaCl solution post detachment (C), Stereomicroscope image of the 6%$_w$-Sodium Oxalate friction material that was in contact with the gray cast iron disc in the 0.1 M NaCl solution post detachment (D).

appears to favor stronger adsorption and a protective layer that primarily reduces anodic current density. EIS analyses confirmed this stronger adsorption for sodium oxalate. Conversely, 2,5-PDA required longer immersion times before forming a crystalline protective precipitate layer, though this layer ultimately appeared more stable during prolonged immersion.

- Stiction tests revealed that the introduction of these inhibitors into the electrolyte drastically reduced the stiction force between the gray cast iron rotor and the friction material, decreasing it from 92 N to approximately 20 N, while also preventing damage to the friction material. Friction materials produced with the incorporation of sodium oxalate at a concentration of 4%$_w$ showed comparable results, whereas a negligible residual stiction force of 11 N was observed for friction materials containing 6%$_w$ sodium oxalate.
- When incorporated directly into the friction material, sodium oxalate suppressed stiction without forming a visually apparent yellow complex on the surface of the gray cast iron disc.

CRediT authorship contribution statement

Michele Motta: Writing – original draft, Methodology, Investigation, Formal analysis, Data curation, Conceptualization. **Agusti Sin:** Funding acquisition. **Lorenzo Fedrizzi:** Validation, Supervision. **Francesco Andreatta:** Validation, Supervision, Project administration.

Declaration of Competing Interest

The authors declare that they have no known competing financial interests or personal relationships that could have appeared to influence the work reported in this paper.

Data Availability

Data will be made available on request.

References

[1] J. Gweon, S. Shin, H. Jang, W. Lee, D. Kim, K. Lee, The factors governing corrosion stiction of brake friction materials to a gray cast iron disc. Brake Colloquium & Exhibition-36th Annual, SAE Technical Paper, 2018, https://doi.org/10.4271/2018-01-1899.

[2] K. Nukumizu, K. Makizono, T. Abe, M. Unno, Influence of rust accumulation on disk rotor on frictional properties of disk brake. 25th Annual Brake Colloquium, SAE Technical Paper, 2007, https://doi.org/10.4271/2007-01-3937.

[3] C.W. Park, M.W. Shin, H. Jang, Friction-induced stick-slip intensified by corrosion of gray iron brake disc, Wear 309 (1-2) (2014) 89–95, https://doi.org/10.1016/j.wear.2013.11.008.

[4] M. Motta, L. Fedrizzi, F. Andreatta, Corrosion stiction in automotive braking systems, Materials 16 (10) (2023) 3710, https://doi.org/10.3390/ma16103710.

[5] P. Sungkhaphaitoon, T. Plookphol, S. Wisutmethangoon, Centrifugal Atomization of Zinc Metal Powder for Friction Materials Application, Adv. Mater. Res. 488 (2012) 281–285, https://doi.org/10.4028/www.scientific.net/AMR.488-489.281.

[6] Lamport, R.A. (2006). *Brake assembly and additive* (U.S. Patent Application No. 11/447,240, Publication No. US 2006/0283673 A1). U.S. Patent and Trademark Office.

[7] M. Motta, V. Iodice, A.S. Xicola, A. Truccolo, L. Fedrizzi, F. Andreatta, Role of copper and zinc additives in the stiction phenomenon of automotive braking systems, Mater. Corros. 75 (8) (2024) 1005–1017, https://doi.org/10.1002/maco.202414322.

[8] M. Motta, M. Zanocco, A. Rondinella, V. Iodice, A. Sin, L. Fedrizzi, F. Andreatta, Inhibitive effect of 8-hydroxyquinoline on corrosion of gray cast iron in automotive braking systems, Electrochim. Acta 449 (2023) 142221, https://doi.org/10.1016/j.electacta.2023.142221.

[9] M. Motta, A. Rondinella, T. Pagnutti, A. Sin, K. Marcoen, K. Baert, F. Andreatta, The Role of Trisodium Phosphate as a Corrosion Inhibitor for Gray Cast Iron in Automotive Braking Systems: Mechanisms and Challenges, Mater. Corros. 76 (12) (2025) 1764–1779, https://doi.org/10.1002/maco.70023.
[10] M. Motta, A. Sin, A. Rondinella, L. Fedrizzi, F. Andreatta, Chitosan as a corrosion inhibitor for gray cast iron and its role in mitigating the stiction phenomenon in automotive braking systems, Electrochim. Acta 555 (2026) 148414, https://doi.org/10.1016/j.electacta.2026.148414.
[11] J.S. Yoo, Y.W. Kim, S.H. Kim, J.G. Kim, Investigation of methods for preventing atmospheric corrosion of gray cast iron brake disc for electric vehicles, Mater. Today Commun. 46 (2025) 112895, https://doi.org/10.1016/j.mtcomm.2025.112895.
[12] T.A. Truc, T.T. Thuy, V.K. Oanh, T.T.X. Hang, A.S. Nguyen, N. Caussé, N. Pébère, 8-hydroxyquinoline-modified clay incorporated in an epoxy coating for the corrosion protection of carbon steel, Surf. Interfaces 14 (2019) 26–33, https://doi.org/10.1016/j.surfin.2018.10.007.
[13] I.B. Obot, N.K. Ankah, A.A. Sorour, Z.M. Gasem, K. Haruna, 8-Hydroxyquinoline as an alternative green and sustainable acidizing oilfield corrosion inhibitor, Sustain. Mater. Technol. 14 (2017) 1–10, https://doi.org/10.1016/j.susmat.2017.09.001.
[14] B. Vaghefinazari, S.V. Lamaka, C. Blawert, M. Serdechnova, N. Scharnagl, P. Karlova, M.L. Zheludkevich, Exploring the corrosion inhibition mechanism of 8-hydroxyquinoline for a PEO-coated magnesium alloy, Corros. Sci. 203 (2022) 110344, https://doi.org/10.1016/j.corsci.2022.110344.
[15] D. Seifzadeh, S. Hamzedoust-Hasankiadeh, A.N. Shamkhali, Electrochemical and DFT studies of 8-hydroxyquinoline as corrosion inhibitor for AZ61 magnesium alloy in acidic media, Prot. Met. Phys. Chem. Surf. 49 (2) (2013) 229, https://doi.org/10.1134/S2070205113020123.
[16] M. Rbaa, M. Fardioui, C. Verma, A.S. Abousalem, M. Galai, E.E. Ebenso, A. Zarrouk, 8-Hydroxyquinoline based chitosan derived carbohydrate polymer as biodegradable and sustainable acid corrosion inhibitor for mild steel: experimental and computational analyses, Int. J. Biol. Macromol. 155 (2020) 645–655, https://doi.org/10.1016/j.ijbiomac.2020.03.200.
[17] M. Rbaa, M. Ouakki, M. Galai, A. Berisha, B. Lakhrissi, C. Jama, A. Zarrouk, Simple preparation and characterization of novel 8-Hydroxyquinoline derivatives as effective acid corrosion inhibitor for mild steel: Experimental and theoretical studies, Colloids Surf. A Physicochem. Eng. Asp. 602 (2020) 125094, https://doi.org/10.1016/j.colsurfa.2020.125094.
[18] M. Galai, M. Rbaa, M. Ouakki, K. Dahmani, S. Kaya, N. Arrousse, M.E. Touhami, Functionalization effect on the corrosion inhibition of novel eco-friendly compounds based on 8-hydroxyquinoline derivatives: experimental, theoretical and surface treatment, Chem. Phys. Lett. 776 (2021) 138700, https://doi.org/10.1016/j.cplett.2021.138700.
[19] M. Rbaa, F. Benhiba, A.S. Abousalem, M. Galai, Z. Rouifi, H. Oudda, A. Zarrouk, Sample synthesis, characterization, experimental and theoretical study of the inhibitory power of new 8-hydroxyquinoline derivatives for mild steel in 1.0 M HCl, J. Mol. Struct. 1213 (2020) 128155, https://doi.org/10.1016/j.molstruc.2020.128155.
[20] X. Liu, Y. Lu, B. Jiang, Electrochemical study on the effect of bipyridine dicarboxylic acid and its cobalt complex on the corrosion behaviour of carbon steel in acidic medium, J. Adhes. Sci. Technol. 29 (6) (2015) 463–472, https://doi.org/10.1080/01694243.2014.994271.
[21] K.R. Ansari, M.A. Quraishi, A. Singh, Corrosion inhibition of mild steel in hydrochloric acid by some pyridine derivatives: An experimental and quantum chemical study, J. Ind. Eng. Chem. 25 (2015) 89–98, https://doi.org/10.1016/j.jiec.2014.10.017.
[22] A.T. Hassan, R.K. Hussein, M. Abou-krisha, M.I. Attia, Density functional theory investigation of some pyridine dicarboxylic acids derivatives as corrosion inhibitors, Int. J. Electrochem. Sci. 15 (5) (2020) 4274–4286, https://doi.org/10.20964/2020.05.11.
[23] I.B. Obot, Z.M. Gasem, Theoretical evaluation of corrosion inhibition performance of some pyrazine derivatives, Corros. Sci. 83 (2014) 359–366, https://doi.org/10.1016/j.corsci.2014.03.008.
[24] U. Rammelt, S. Koehler, G. Reinhard, Electrochemical characterisation of the ability of dicarboxylic acid salts to the corrosion inhibition of mild steel in aqueous solutions, Corros. Sci. 53 (11) (2011) 3515–3520, https://doi.org/10.1016/j.corsci.2011.06.023.
[25] G. Reinhard, M. Radtke, U. Rammelt, On the role of the salts of weak acids in the chemical passivation of iron and steel in aqueous solutions, Corros. Sci. 33 (2) (1992) 307–313, https://doi.org/10.1016/0010-938X(92)90154-U.
[26] A. Hoyt, S. Li, X. Dai, C. Garcia, H. Cong, B.M. Zhang Newby, Synergistic effect of pH and oxalate concentration on corrosion of aluminium alloy 2024-T3, Corros. Eng. Sci. Technol. 53 (6) (2018) 413–421, https://doi.org/10.1080/1478422X.2018.1495678.
[27] P. Satyabama, S. Rajendran, T.A. Nguyen, Corrosion inhibition of aluminum by oxalate self-assembling monolayer, Anti-Corros. Methods Mater. 66 (6) (2019) 768–773, https://doi.org/10.1108/ACMM-01-2019-2061.
[28] E.J. Low, H.M. Yusoff, N. Batar, I.N.Z. Nor Azmi, P.W. Chia, S.S. Lam, M.F. Ridwan Zulkifli, The use of food additives as green and environmental-friendly anti-corrosion inhibitors for protection of metals and alloys: a review, Environ. Sci. Pollut. Res. 30 (31) (2023) 76297–76307, https://doi.org/10.1007/s11356-023-27823-3.
[29] L. and P.Cavallotti. Paracchini, "Manuale di trattamenti e finiture. Handbook of treatments and finishes," 1st ed., Tecniche Nuove, Milan, 2003.
[30] L. Kobotiatis, N. Pebere, P.G. Koutsoukos, Study of the electrochemical behaviour of the 7075 aluminum alloy in the presence of sodium oxalate, Corros. Sci. 41 (5) (1999) 941–957, https://doi.org/10.1016/S0010-938X(98)00164-4.
[31] C. Giacomelli, F.C. Giacomelli, J.A.A. Baptista, A. Spinelli, The effect of oxalic acid on the corrosion of carbon steel, Anti-Corros. Methods Mater. 51 (2) (2004) 105–111, https://doi.org/10.1108/00035590410523193.
[32] T. Pastore, M. Cabrini, L. Coppola, S. Lorenzi, P. Marcassoli, A. Buoso, Evaluation of the corrosion inhibition of salts of organic acids in alkaline solutions and chloride contaminated concrete, Mater. Corros. 62 (2) (2011) 187–195, https://doi.org/10.1002/maco.201005789.
[33] I. Sekine, C. Okano, Corrosion behavior of mild steel and ferritic stainless steels in oxalic acid solution, Corrosion 45 (11) (1989) 924–932, https://doi.org/10.5006/1.3585002.
[34] G. Monari, M. Galeotti, M. Matteini, B. Salvadori, R. Stifanese, P. Traverso, P. Letardi, Protective treatments for copper alloy artworks: preliminary studies of sodium oxalate and limewater effectiveness against bronze disease, Environ. Sci. Pollut. Res. 30 (10) (2023) 27441–27457, https://doi.org/10.1007/s11356-022-24107-0.
[35] W. Su, J.O. Iroh, Electropolymerization of pyrrole on steel substrate in the presence of oxalic acid and amines, Electrochim. Acta 44 (13) (1999) 2173–2184, https://doi.org/10.1016/S0013-4686(98)00343-0.
[36] A. De Bruyne, J.L. Delplancke, R. Winand, Comparison between polypyrrole films obtained on mild steel by electropolymerization from oxalic acid and sodium sulphate aqueous solutions, Surf. Coat. Technol. 99 (1-2) (1998) 118–124, https://doi.org/10.1016/S0257-8972(97)00417-9.
[37] S. Goidanich, L. Brambilla, L. Mathys, R. Pellicanò, L. Maghini, A. Brenna, E. Joseph, Effetto di pulitura e biopassivazione su acciaio Corten, La Metall. Ital. 14 (2023).
[38] L.I. Fockaert, T. Würger, R. Unbehau, B. Boelen, R.H. Meißner, S.V. Lamaka, J.M.C. Mol, ATR-FTIR in Kretschmann configuration integrated with electrochemical cell as in situ interfacial sensitive tool to study corrosion inhibitors for magnesium substrates, Electrochim. Acta 345 (2020) 136166, https://doi.org/10.1016/j.electacta.2020.136166.
[39] S.V. Lamaka, B. Vaghefinazari, D. Mei, R.P. Petrauskas, D. Höche, M. L. Zheludkevich, Comprehensive screening of Mg corrosion inhibitors, Corros. Sci. 128 (2017) 224–240, https://doi.org/10.1016/j.corsci.2017.07.011.
[40] Sin Xicola, A., Fedrizzi, L., Andreatta, F., & De Nicolo, A. (2022). *Method and equipment for determining conditions of stiction between a braking element and an element to be braked* (U.S. Patent No. 12,025,551). U.S. Patent and Trademark Office.
[41] H.G.M. Edwards, N.C. Russell, Vibrational spectroscopic study of iron (II) and iron (III) oxalates, J. Mol. Struct. 443 (1-3) (1998) 223–231, https://doi.org/10.1016/S0022-2860(97)00390-6.